Journal of Materials Processing Technology 216 (2015) 206–215

Contents lists available at ScienceDirect

Journal of Materials Processing Technology

journal homepage: www.elsevier.com/locate/jmatprotec

A force controlled grinding-milling technique for quartz-glass micromachining

Shun-Tong Chen*, Zong-Han Jiang

Department of Mechatronic Engineering, National Taiwan Normal University, Taiwan

ARTICLE INFO

Article history:
Received 23 February 2014
Received in revised form 8 September 2014
Accepted 19 September 2014
Available online 28 September 2014

Keywords:
Ductile regime machining
Intellectualized grinding-milling technique
Double-negative back rake angle (DN-BRA)

ABSTRACT

This paper presents a novel approach to the micromachining of quartz glass using an intellectualized grinding-milling technique to overcome the difficulties in machining hard-brittle materials. A bench-type linear 3-axis CNC machine tool providing grinding-milling at depths of several nanometers is constructed to realize ductile-regime material removal during quartz-glass milling. Finite element analysis (FEA) is conducted on the deformation and resonant frequency of the developed machine tool. A micro-tipped grinding-tool made of boron-doped polycrystalline composite diamond (BD-PCD) and designed with a double-negative back rake angle (DN-BRA) to create compressive stress grinding-milling is proposed and employed. To sense the force at which grinding-milling is conducted and provide real-time feedback on the milling tool's feed-rate, load-cells are devised on 3 axes. Using an appropriate grinding-milling technique in combination with proper feedback to control the machining feed-rate, quartz glass is machined layer-by-layer under a ductile regime. A miniature 3-step-shaped pyramid made of quartz glass of 0.3 mm in height and of Ra0.66 μm surface roughness with very little brittle fracturing is achieved. The optimum grinding depth, milling speed and corresponding grinding-milling force are 1 μm, 50–70 m/min, and 0.4 N, respectively. A comprehensive examination of the quantitative and qualitative properties of the BD-PCD tool was undertaken. Experimental confirmation of the proposed approach is presented. Additionally, the following aspects are discussed in detail: the spark erosion rate of the machined diamond tool, milling feed-rate, grinding depth, graphitization of diamond, and tool wear.

1. Introduction

The trend toward miniaturization of consumer and industrial products is inevitable. This trend is presently realized in lightweight, miniaturized products of high functionality. Optical glass such as quartz glass is widely used in laboratory glassware, optical instruments, semiconductors and precision equipment. This is due to its exceptional transmission ability in both ultraviolet and infrared spectra, good corrosion resistance, high compressive strength, and excellent wear-resistant properties. Table 1 lists the mechanical properties of quartz glass.

Quartz glass, however, is a difficult to machine brittle material. Its many positive attributes and uses mean precision machining of quartz glass has attracted much research and many techniques have been proposed and tested. These include the use of laser-beam machining, water-jet assisted laser-beam machining, ultrasonic machining, and electrochemical methods. Each method has its merits and limitations. Laser-beam machining is a widely used thermal process where absorbed optical energy is converted to heat energy to facilitate cutting. Dubey and Yadava (2008) pointed out that this process leaves tapers on the machined kerf of components due to the converging-diverging shape of laser beams. Hildebrand et al. (2012) employed a CO_2-laser to polish quartz-glass parts. They found that the technology was successful but that it was limited by heat developing during polishing and that a suitable cooling process was necessary to reduce material tensions. Hock et al. (2012) used a water-jet guided fiber laser to cut thin metal sheets. This technique allowed for reflection at the air-water interface to suppress tapering of the cut kerf. The machining process while successful in reducing tapering took much longer than conventional laser-beam cutting. Ultrasonic vibration-assisted machining utilizes ultrasonic vibration superimposed on the movement of the cutting tool converting its continuous cutting motion into a multiple impact process. This approach can be used for machining brittle material; however, Guzzo et al. (2003) noted that material removal resulted from a brittle micro-cracking mechanism, implying potential subsurface damage to the quartz. Electrochemical spark machining (ECSM) combining both electrochemical and electrical discharge

* Corresponding author. Tel.: +886 277343510.
E-mail addresses: chenst@ntnu.edu.tw, chenst@ntu.edu.tw (S.-T. Chen).

http://dx.doi.org/10.1016/j.jmatprotec.2014.09.017
0924-0136/

Table 1
The physical properties of quartz glass.

Density (g/cm^3)	2.2
Young's modulus (GPa)	71.6
Poisson's ratio	0.17
Torsional rigidity	31.4
Compression strength (GPa)	1.1
Bending strength (MPa)	69
Tensile strength (MPa)	55
Vickers hardness (Gpa)	8.8–10.1

machining can be successfully used for machining quartz glass (Jain and Adhikary, 2008); however, the employed chemicals and chemical wastewater are hazardous to the environment.

As stated, due to its excellent physical properties, quartz glass is employed widely in various fields. It is used as cells in spectrophotometers (both clear and masked with black quartz to block off-axis rays), small quartz flasks, quartz furnace tubes, quartz bell jars, small quartz crucibles and so on. However, it is 8.8–10.1 (Gpa) on the Vickers hardness scale and machining such hard-brittle material is difficult. Tools made of tungsten carbide, ceramic oxide, and cubic boron nitride (CBN) are not suitable for cutting such material. On the other hand, mono-crystalline diamond tools have both the hardness and edge smoothness to cut quartz glass. Such a tool creates excellent dimensional accuracy and surface finish; however, its production is expensive and sophisticated. A feasible alternative tool is one made from less expensive boron-doped synthesized diamond (termed BD-PCD). Kalish (2001) showed that boron with one less electron than carbon and small atomic radius is relatively easily incorporated into diamond. Ekimov et al. (2004) discussed boron acting as a charge acceptor when diamond is doped with boron resulting in the diamond structure being effectively hole-doped. The great advantage of the BD-PCD is its electrical conductivity which allows diamond grains to be easily cut (broken) by spark erosion. This means the diamond edge can be meticulously manipulated to give a tool of excellent qualities. Moriyoshi et al. (1982) observed that the boundary between particulate diamond grains revealed D–D (diamond–diamond) bonding under formation conditions of high pressure and temperature. For micromachining, a grain size of 5–10 μm is enough to minimize the gap between diamond grains and expose a suitable diamond grinding-edge. Table 2 lists the ingredients of BD-PCD (Suzuki et al., 2009).

Having comprehensively surveyed existing technologies used in hard-brittle material machining, it is evident that maintaining dimensional and geometrical accuracy is an important but as yet inadequately resolved issue. Based on previous research (Chen and Chang, 2013), this work focuses on the feasibility of successfully machining quartz glass economically without brittle fracturing. A reliable, environmentally friendly, highly precise approach to the machining of 3-D microstructures on quartz glass is developed. A micro-edged grinding-tool made of BD-PCD, possessing a pair of DN-BRA to create compressive stress at the machined surface of quartz glass is designed and employed. Approaches to PCD tool formation, determination of critical grinding depth, and feedback control of grinding-milling force as well as tool wear are all evaluated.

Table 2
The ingredients of BD-PCD.

Ingredients	Conditions
Type of PCD	Boron-doped HPHT diamond
Thermal conductivity	440–580 W/m K
Grain size	5–10 μm
Bond	Cobalt
Resistivity	5–37 × 10 Ωm

Table 3
Specifications of the three translation stages.

	X-axis	*Y*-axis	*Z*-axis
Travel (mm)	50	50	25
Resolution (nm)	1	1	4.5
Straightness (nm)	±75	±75	±300
Repeatability (μm)	±1	±1	±3

2. Methodology

2.1. Ductile grinding mechanism of hard-brittle material

As the cutting depth is shallow, transition from brittle to ductile grinding occurs during material machining. The cutting depth which leads to material removal during the plastic deformation process is termed the 'critical cutting depth d_c'. A prediction of the brittle–ductile transition mechanism for a critical cutting depth d_c was proposed by Bifano et al. (1991) as follows:

$$d_C = 0.15 \times \left(\frac{E}{H}\right)\left(\frac{K_C}{H}\right)^2 \quad (1)$$

where E is the elastic modulus, K_c is fracture toughness, and H is the hardness of hard-brittle material. The critical cutting depth for fracture initiation is directly proportional to the elastic modulus and fracture toughness of brittle material. Therefore, brittle material removal can be conducted little-by-little at an appropriate cutting depth. High system rigidity helps reduce deformation of the structural body of the workpiece under the influence of machining forces and the static weight of the machine structure itself. Fig. 1(a) illustrates the removal mechanism of hard-brittle material under ductile machining. Blackley and Scattergood (1991) considered fracturing when the effective critical cutting depth propagated to a surface damage depth of y_c as shown in Fig. 1(b). Under a ductile grinding regime, machining can be implemented as micro fracturing does not extend below the cut surface plane.

2.2. Construction of an intellectualized compact grinding-milling machine

To achieve cost-effective high-precision machining of a 3-D microstructure on quartz glass, an intellectualized compact grinding-milling machine with a self-regulating feed-rate is designed and constructed in this work. The intellectualized machine is equipped with three precision linear translation stages and a horizontal high-speed spindle. It can support nanometric-scale feed resolution to achieve ductile regime machining on hard-brittle material as shown in Fig. 2(a). In addition, it is also provided with a set of sensitive load-cells allowing for the milling-grinding force to be detected along 3 axes providing a mechanism for feedback to regulate in real time the milling feed-rate. The low-gravity design increases system rigidity and minimizes Abbe errors to improve machining accuracy. Horizontal milling-grinding benefits microchip disposal while an electronic direct drive linear motor provides drive with neither backlash nor wear, which supports sudden real-time feed-rate corrections. Table 3 lists the specifications of the three linear stages (Aerotech, Inc., 2012). Fig. 2(b) presents a finished prototype of the compact CNC machine tool.

2.3. Proposed feedback control loop design and structural analysis

Total grinding energy consists of sliding, plowing, and grinding (Amitay et al., 1981). Consequently, grinding-milling is treated as a combination of sliding, plowing, grinding, and milling (layer-by-layer) according to a schemed CNC pathway. Under ideal machining conditions, the grinding-milling process can create a 3D-shaped

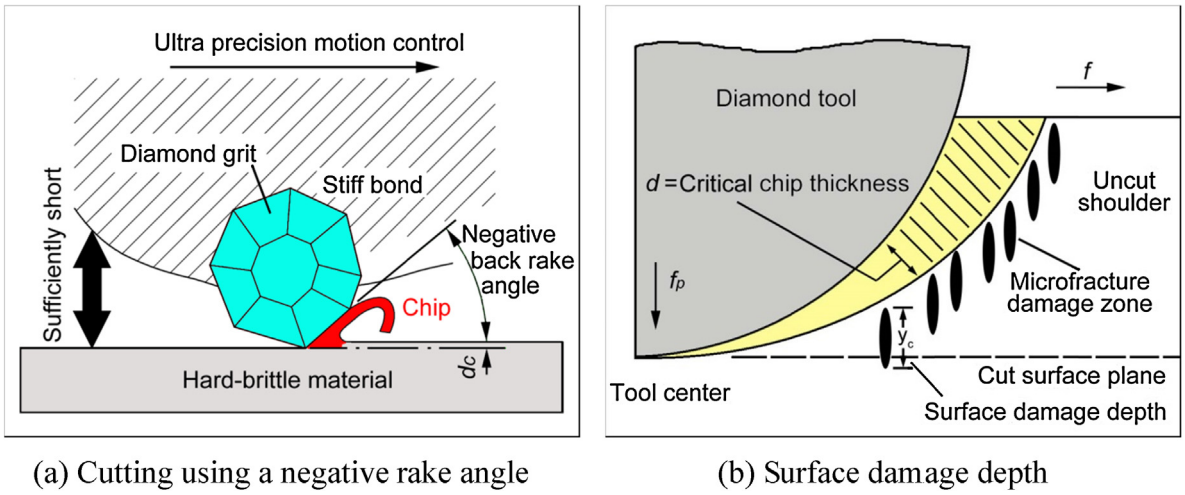

Fig. 1. Ductile regime machining on hard-brittle material.

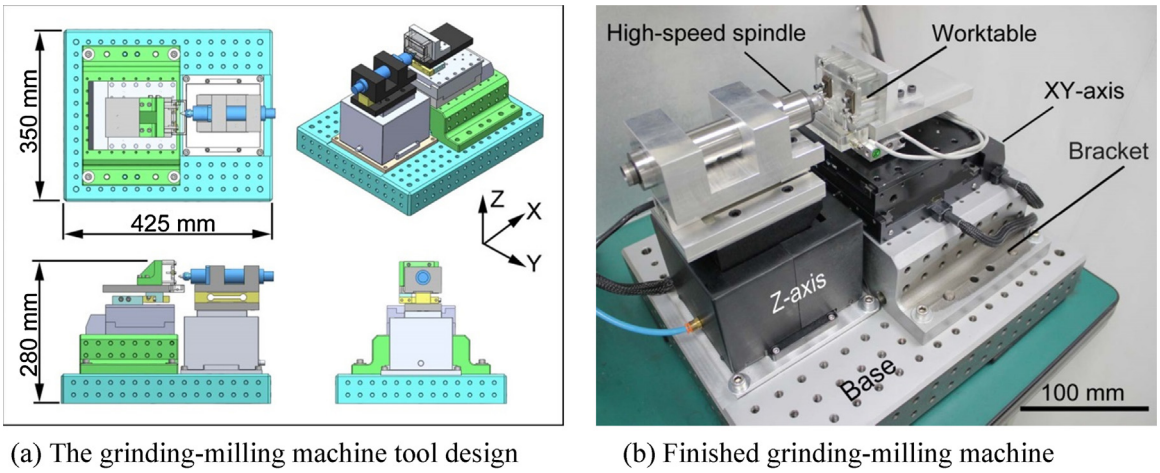

Fig. 2. Construction of the intellectualized compact grinding-milling machine.

structure using an end diamond grinding-tool. An appropriate constant machining force giving superior performance and preventing brittle fracturing is essential. Hence, in this study, the installation of individual load-cells inside the *X*-, *Y*- and *Z*-axes' stages to provide feedback on grinding force is developed. These load-cells continuously sense machining force once grinding-milling has started (Fig. 3(a)). Real-time analog voltage is converted to digital data through an A/D converter before PC input, and then compared with

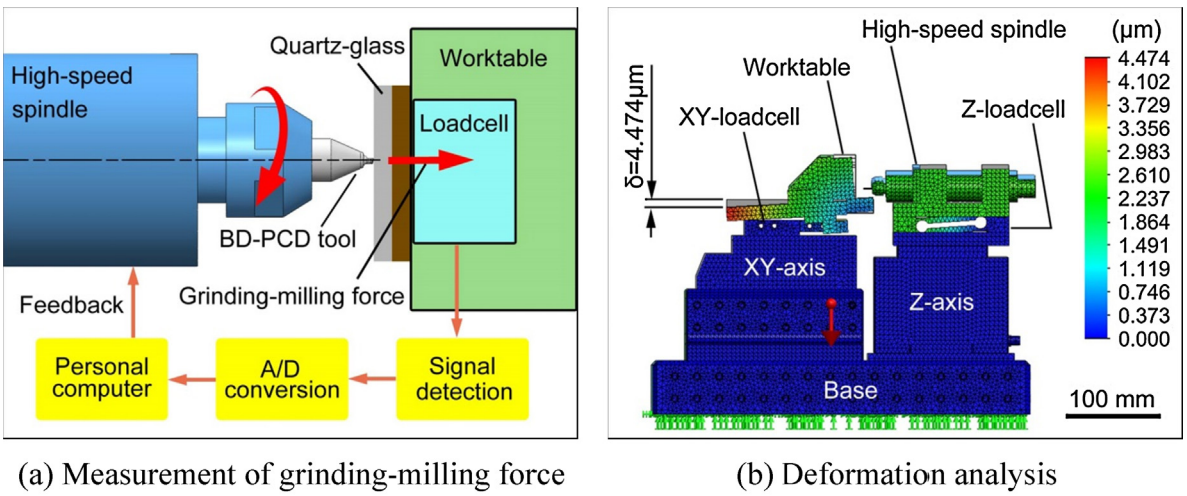

Fig. 3. Proposed feedback control loop design and structural analysis.

a predetermined voltage, which corresponds to the appropriate grinding-milling force at which brittle fracturing does not occur. The real-time corrected feed-rate is immediately fed back to the tool to ensure an appropriate grinding-milling force. The designed machine's high rigidity is *sine qua non* conditions to prevent deformation and maintain machining accuracy during grinding. Utilizing Finite Element Method (FEM) to analyze the relative merits of the entire structural design, a maximum constant deformation δ of 4.5 μm at the end of the structural body of the *XY*-worktable under deadweight is found (Fig. 3(b)). Such errors can be corrected through internal compensation. In addition, system resonance is found to occur at 131.2 Hz. This means operation on the machine must occur at a frequency removed from its own natural resonance frequency to avoid vibration.

3. Experimental approach

3.1. Design of a micro grinding-tool with double-negative back rake angle

Brittle material has a very low elongation percentage, which causes failure with little deformation. This indicates that tensile strength is much less than compressive strength. As a result, material removal is proposed under a compressive loading regime so as to avoid brittle fracturing during machining. A micro end grinding-tool with a double-sided negative back rake angle is designed (Fig. 4(a)-(1)). With consideration given to both tool strength and escaping chips, a back rake angle of −60° between the tool's centerline and the inclined plane is recommended (Chen et al., 2011). That is, the grinding-edge is tilted at 30° with respect to the machined surface. Negative angle machining prompts material removal under a press-cut regime, creating compressive stress on the hard-brittle material, which radically reduces micro cracking and fracturing. Furthermore, the symmetrical negative-angle design benefits bi-directional rotational grinding and chips escaping. To predict how the design will work under real conditions, a hypothetical force of 1N is acted on the lateral of the grinding-milling tool and stress analysis of the designed tool is performed. See Fig. 4(a)-(2) for the results of 1N loading deformation. Maximum deformation of about 1.1 μm occurred at the outside-end corner of the tool. This is an acceptable level for the milling-grinding process. w-EDM (wire cut electric discharge machining) is used to form the tool using one pass for roughing and two passes for finishing. Usage of low discharge energy is helpful in reducing degeneration at the surface layer from occurring and ensures a tool with a more exact edge width. Table 4 lists the machining conditions for the formation of the BD-PCD tool. Note that removing the shaft-core portion of the tool's end-face can prevent squeezing between the workpiece material and center of the tool due to no cutting speed at this point (Fig. 4(a)-(3)). Fig. 4(b) shows the finished micro end grinding-tool with DN-BRA.

Table 4
Conditions for formation of the end grinding-tool.

Parameters	Roughing	Finishing (×2)
Servo voltage (V)	65	65
On time (μs)	2	2
Off time (μs)	15	16
Auxiliary on time (μs)	1	1
Auxiliary off time (μs)	15	16
Wire speed (mm/s)	7	7
Wire tension (N)	20	20
Diameter of wire (mm)	0.25	0.25
Water pressure (N/cm^2)	10	10
Spindle speed (rpm)	500	500

3.2. Effect of back rake angle

For comparison purpose, a preliminary grinding-milling experiment on the effect of the back rake angle is conducted on quartz glass (grinding speed: 70 m/min, milling feed-rate: 120 mm/min, grinding depth: 1 μm/layer, total depth: 10 μm and oil mist). Fig. 5 shows the tentative results of the resultant surface using BRAs of −90° and −60°, respectively. Evidently, brittle fracturing is generated at a BRA of −90°, termed brittle regime grinding-milling (Fig. 5(a)). Due to a lack of an appropriate BRA, chips cannot escape, leading to repeated and continuous squeezing, friction, and scraping between grinding-edges and the machined surface thus causing brittle fracturing. By contrast, a −60° BRA creates ductile regime grinding-milling and an even machining surface with fine and regular tool mark impressions (Fig. 5(b)). A negative BRA facilitates chip discharge due to the relief angle between the grinding edge and machined surface. Additionally, a negative BRA makes brittle material bear depression forces resulting in improved material removal under a compressive stress regime. Lastly, the finished tool is not unloaded and repositioned on the spindle until all tasks are completed. These strategies minimize potential brittle fracturing.

3.3. Setup of load-cells

To accurately measure resistance from the employed load-cell, a Wheatstone bridge circuit is conducted in the experiment. When

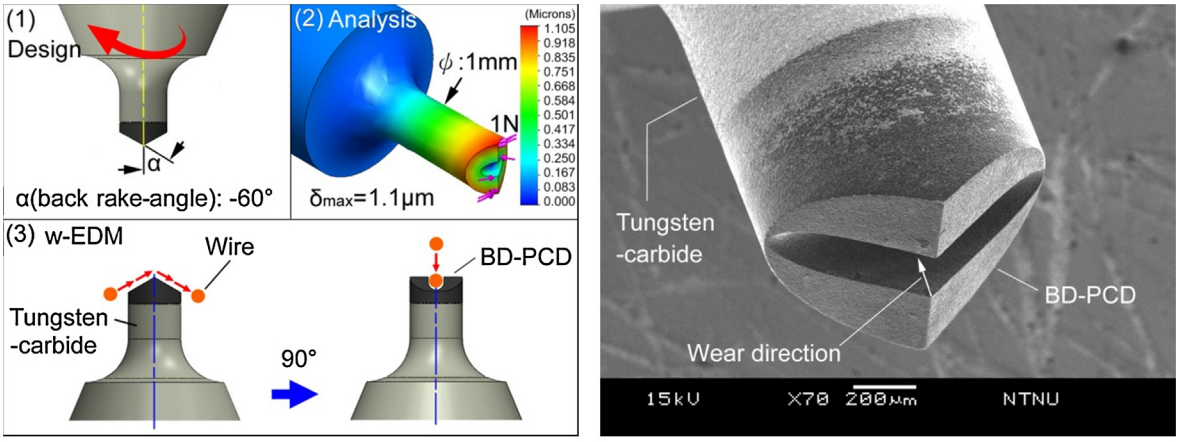

(a) Negative back rake angle design (b) Finished end grinding-tool

Fig. 4. Design of the micro end grinding-tool with DN-BRA.

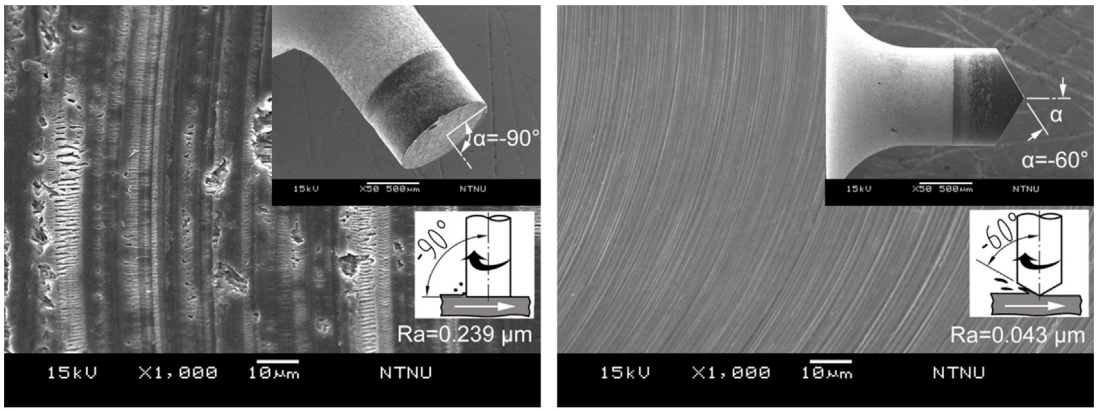

(a) BRA at α=-90° (b) BRA at α=-60°

Fig. 5. Comparison of surface integrity '*without*' and '*with*' negative BRA.

a load-cell has no loading, the four gauges are at rest and have the same ohm value R as described in Eq. (2), which denotes the bridge is balanced and the output voltage V_o is zero. When loading the load-cell, the Wheatstone bridge converts the gauge's strain-induced resistance changes into a differential voltage. Hence, any very small changes in resistance ΔR can be measured from the strain gauges placed in the arms of the bridge: R_1, R_2, R_3 and R_4. The output voltage V_o for the applied force is expressed in Eq. (3),

$$R_1 = R_2 = R_3 = R_4 = R \tag{2}$$

$$V_o = \left[\frac{R_4}{R_3 + R_4} - \frac{R_2}{R_1 + R_2}\right] \times V_{ex} \tag{3}$$

Combining a load-cell with a precision motion stage as the sensor mechanism allows for constant detection of the machining force and the provision of a real-time feedback. This feedback force plays an important role in the rapid regulation of the grinding-tool's feed-rate to ensure continuous ductile regime machining. Fig. 6(b) illustrates an experimental arrangement for grinding-milling force detection. The distribution of load-cells is helpful in saving assembly space and maintaining the structural rigidity of such a compact machine. To enhance the signal-to-noise ratios (SNR) and obtain greater accuracy, amplifications and calibrations of on-machine signals for zeroing load-cells are conducted. The maximum and minimum loading range of the load-cells along the X-, Y- and Z-axes are X_{max}: 50 N, X_{min}: 0.002 N, Y_{max}: 50 N, Y_{min}: 0.002 N, Z_{max}: 100 N, Z_{min}: 0.002 N, respectively.

3.4. Feedback control of grinding-milling force

To avoid improper grinding-milling forces leading to brittle fracturing or excessive friction on the quartz-glass, an algorithm for deciding the correct grinding-milling force is established. As suggested in Eq. (4), exact judgment of whether the detected milling-grinding force is over the critical machining force is essential. The feedback control loop controls the tool feed-rate by slowing or speeding up grinding. The feed-rate returns to zero and recounts in real time when the difference between the milling-grinding detected force (F_m) (only Z-axis) and the average accumulated force (F_t) are greater than that of a predetermined (F_s) benchmark value. Otherwise the feed-rate increases successively by 20% to a maximum of 200%. This process enhances machining performance.

$$F_m - \frac{\sum F_t}{A_t} \geq F_s \tag{4}$$

where A_t is the accumulated cycle times in milling-grinding force detecting. An initial tool feed-rate of 150 mm/min is given as the F_s to confirm the feasibility of Eq. (4). Fig. 7 presents the comparison of preliminary experimental results between '*with*' and '*without*' feedback control and SEM images. Note the curve that represents the real-time milling-grinding force in the Z-axis goes up gradually

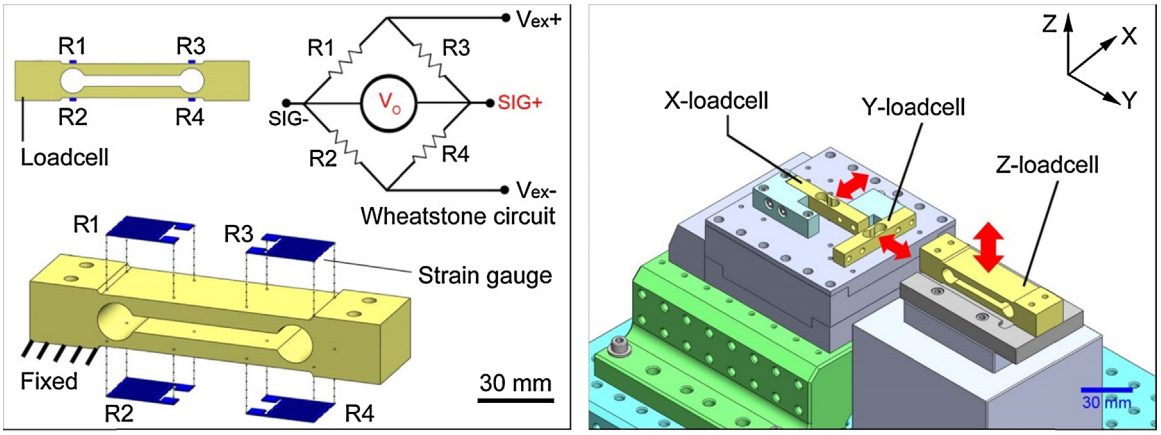

(a) Wheatstone bridge circuit in load-cell (b) Installation of the load-cells

Fig. 6. Setup for the load-cells.

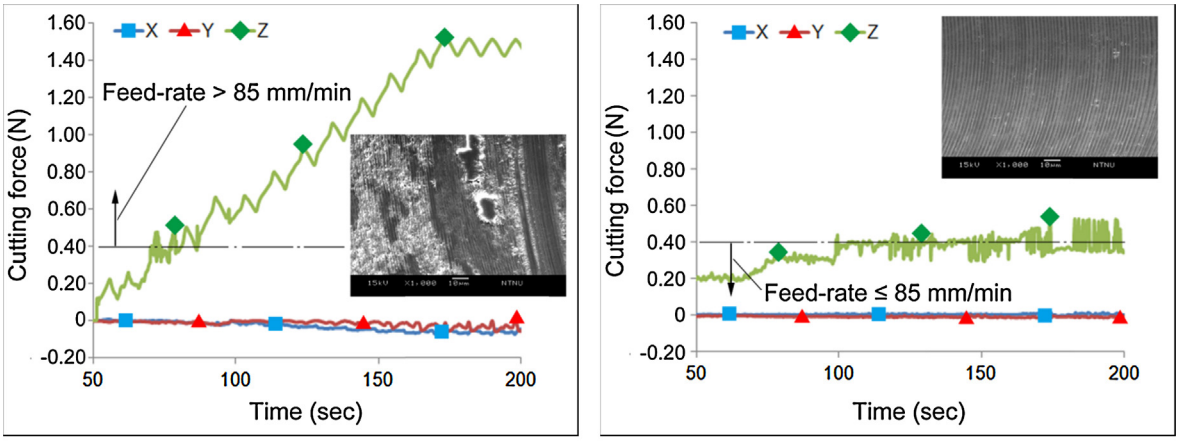

Fig. 7. Comparison of experimental results between '*with*' and '*without*' feedback control.

(up to 1.6 N) when the feedback control loop is disabled. Excessive machining force results in a feed-rate which leads to brittle fracturing on the machined surface (Fig. 7(a)). Corresponding surface roughness is obtained at Ra0.099 μm. By contrast, when the feedback control loop is enabled, the curve becomes relatively flat. With increased grinding-milling force, the tool's feed-rate dwindles down to 85 mm/min. This helps maintain a ductile machining regime. The appropriate milling-grinding force is about 0.4 N which produces a surface roughness of Ra0.056 μm (Fig. 7(b)). Experimental results demonstrate that the self-regulating feed-rate improves machining performance via the designed feedback control loop.

4. Verification

In this section, a miniature 3-step-shaped pyramid made of quartz glass is machined to verify the feasibility of the proposed approaches. The pyramid is 0.3 mm in total height and

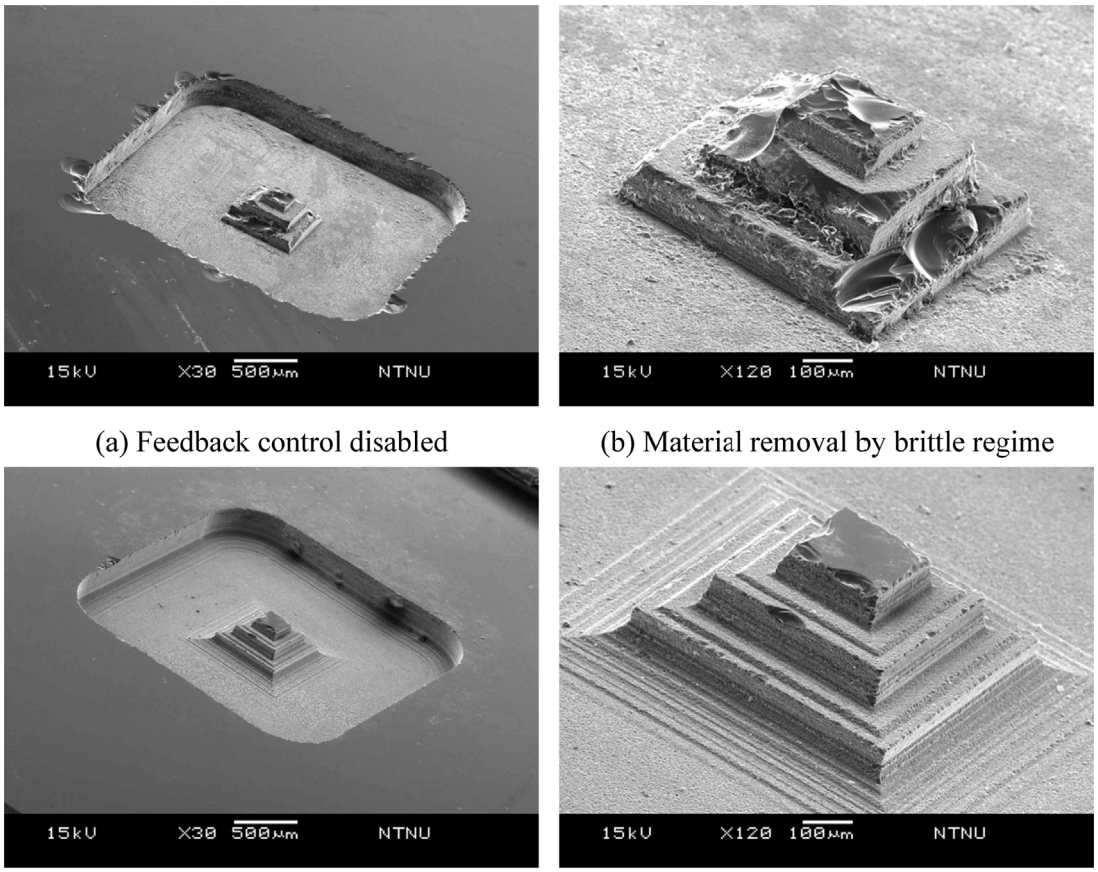

Fig. 8. The miniature 3-step-shaped pyramid grinding-milling on quartz-glass.

Table 5
The grinding-milling conditions.

Parameters	Conditions
Tool	BD-PCD
Work-piece	Quartz-glass
Grinding speed (V)	70 m/min
Initial feed-rate (F)	150 mm/min
Grinding depth (D_c)	1 μm/layer
Coolant	Oil mist
Feedback control	Disenabled/enabled

square 0.2 mm on side length of the top-step. The grinding-milling of the steps of the pyramid are implemented '*with*' and '*without*' feedback control of the grinding-milling force according to a predetermined CNC pathway. Table 5 lists the grinding-milling conditions. The initial tool feed-rate and grinding depth are 150 mm/min and 1 μm/layer, respectively. No feedback control exists over grinding-milling force when grinding-milling resistance detection is disabled (Fig. 8(a) and (b)). If the feed-rate is too fast, material is squeezed and plowed as there is too little time for material removal. A phenomenon similar to transgranular fracturing then occurs (Astakhov, 1999). The machining time for completing the miniature pyramid was only 40 min (including the pocket and pyramid paths). When grinding-milling resistance detection is enabled, feedback slows the milling process to meet the critical force needed for successful grinding. The appearance of additional steps is caused by a rougher CNC pathway scheme. However, brittle fracturing is greatly suppressed and a better milling outcome is achieved (Fig. 8(c) and (d)). Note that the machining time was 70 min; however, this is compensated for by high geometrical and dimensional accuracy and excellent surface roughness on the miniature steps of the miniature pyramid can be achieved.

5. Discussions

5.1. Influence of discharge energy on formation of BD-PCD tool

BD-PCD conducts electricity due to electron-holes in its diamond lattice (Chen and Chang, 2013) while tungsten carbide conducts electricity by free flowing electrons. BD-PCD tool consists of polycrystalline composite diamond and a tungsten carbide substrate. The differences in electrical conductivity between substrate and the polycrystalline diamond edge create spark erosion issues when w-EDM is used for cutting tool edges. If cutting proceeds from tungsten carbide to PCD, the feed-rate of the brass wire becomes very slow and may even stall at the interface. This results from a sharp reduction in conductivity, abruptly reducing the rate of spark erosion. This anomaly potentially increases the probability of a discharge short circuit and even graphitization of diamond grains. It occurs because discharge conditions are initially set according to the demands of tungsten carbide, which has a higher conductivity than BD-PCD. As a result, a micro notch circle is generated (Fig. 9(a)). Besides the above graphitization of diamond grains, this process also affects the formation of the grinding-milling tool. By contrast, when the brass wire works from PCD to tungsten carbide, a sudden increase in the amount of electrons available at the interface occurs and the spark erosion rate increases. In this case cutting progresses more favorably and moves through the interface without the occurrence of notch circles (Fig. 9(b)).

5.2. Critical grinding-milling depth

The native property of quartz glass as a brittle material readily reveals brittle fracturing during machining. This greatly affects surface topography. Different grinding-milling depths give different surface topographies. Fig. 10(a) shows the experimental results corresponding to the surface topographies for different levels of grinding depth in 1–4 μm, respectively. Obviously, grinding-milling with a grinding depth of 1 μm creates a desirable fine surface (see Fig. 10(a)-(1)). This indicates that such a grinding depth accomplishes a ductile machining regime on quartz glass. Extending the grinding depth to 2 μm increases material removal; however, brittle fracturing begins to appear (see Fig. 10(a)-(2)). Further extension of the grinding depth to 3 μm aggravates this phenomenon (see Fig. 10(a)-(3) and (4)). On the basis of the above experiments, a grinding depth of 1 μm is employed as the critical grinding-milling depth (d_c) on quartz glass throughout this study. Correspondingly, a surface roughness down to a level of Ra0.025 μm can be achieved (Fig. 10(b)). This was measured using a laser scanning confocal microscope. The top-left and -right pictures of Fig. 10(b) are the sampling area and surface topography scans of the machined surface, respectively.

5.3. The grinding speed

Grinding speed (V) is defined as instantaneous velocity as a diamond-grit passes through a ground point on a workpiece. Significant correlation exists between grinding speed and surface roughness. Four candidate grinding speeds: 30, 50, 70 and 90 m/min are tested to examine their influence on the machined surface. (The initial tool feed-rate: 120 mm/min, grinding depth: 1 μm/layer, total depth: 10 μm and oil mist). Grinding-milling with a diamond abrasive on quartz glass leads to friction, plowing, and grinding

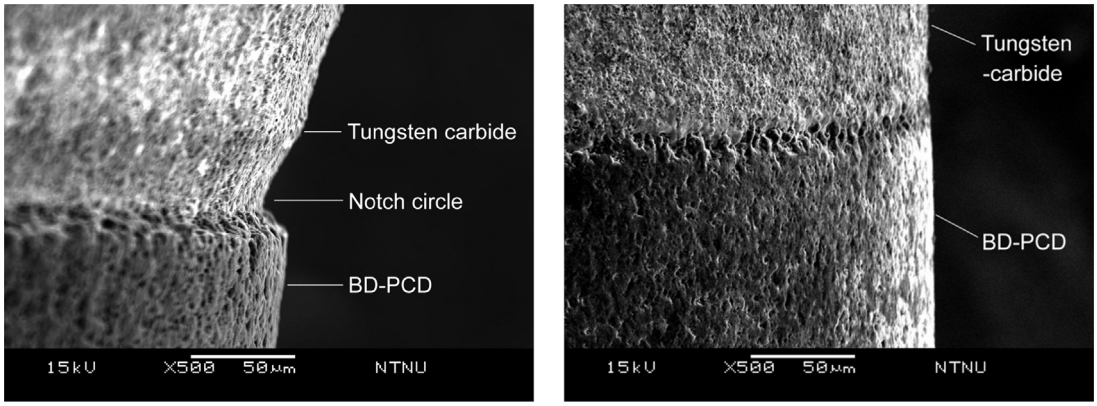

(a) Cutting from tungsten carbide to PCD (b) Cutting from PCD to tungsten carbide

Fig. 9. Influence of discharge energy on the formation of BD-PCD tool.

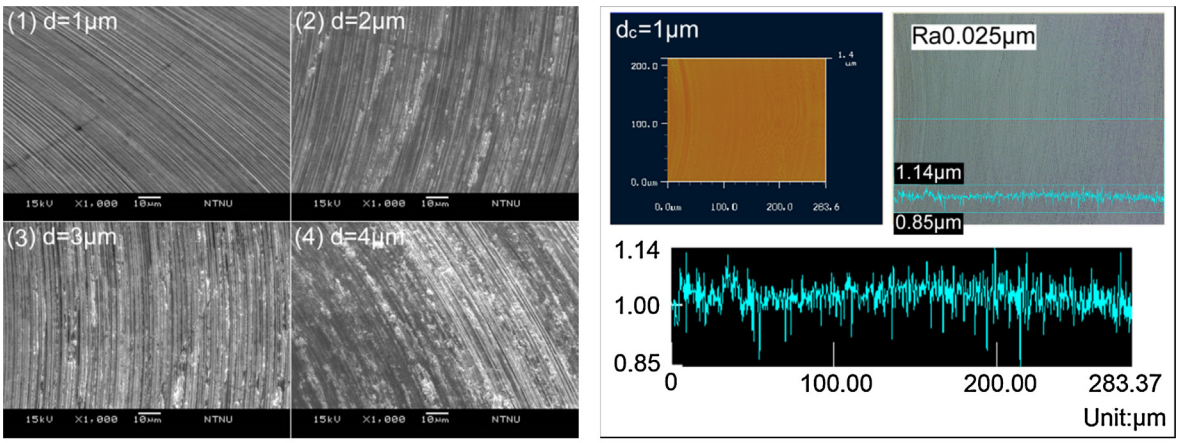

(a) Effect of grinding-milling depth (b) Surface roughness at d_c=1μm

Fig. 10. Relationship between grinding-milling depth and surface roughness.

during removal. The lowest surface roughness is Ra0.043 μm for a grinding speed of 30 m/min (Fig. 11(a)-(1)). However, the grinding mechanism is less than friction, causing an extremely low material removal rate. At lower grinding speeds less abrasive kinetic energy is made available, suggesting that machining resistance results in material removal being more difficult. Increasing the grinding speed to 50 m/min can completely remove material without brittle fracturing (Fig. 11(a)-(2)). It is inferred from this that such a speed produces enough kinetic energy to allow ductile grinding-milling. When grinding speed increases to 70 m/min, a few brittle fractures are generated by slight system vibration (Fig. 11(a)-(3)). Grinding speed at 90 m/min further worsens surface roughness due to increased system vibration. It does, however, improve grinding efficiency (Fig. 11(a)-(4)). Therefore, grinding speeds of 50–70 m/min are selected for this study. The corresponding surface roughness is obtained at Ra0.139 μm (Fig. 11(b)).

5.4. Graphitization and wear of the designed diamond tool

While BD-PCD has higher electrical conductivity than standard PCD, its diamond structure can still be catalyzed to sp^2 structure above 800 °C (Sung and Tai, 1997). Therefore w-EDM can lead to surface degeneration at the grinding-edge of the diamond tool. Analysis of three different B-doped-PCD-tool structural surfaces using Raman spectra was conducted. These are represented in Fig. 12(a) below. The blue curve represents Raman spectra of the original BD-PCD tool surface. The red curve shows Raman spectra of the same tool after roughing and finishing while the purple curve gives the spectra after the too1 was used for cutting quartz glass. In the original case a very strong Raman spectra peak was found at about 1334 cm^{-1}. After roughing and finishing with w-EDM, two weak peaks for non-diamond carbon appear at about 1334 cm^{-1} and 1584 cm^{-1}, respectively. These peaks are typical of sp^2 graphite structures. Graphitization is predictable since spark erosion causes local temperatures up to 12,000 °C (Sommer, 2000). When using w-EDM to finish the diamond edge of a tool, it is possible to reduce graphitization of the surface degeneration layer by reducing the discharge energy used. However, a study by Deng et al. (2011) showed that appropriate graphitization can play an important role as a solid lubricant during machining. This can reduce friction and wear of the diamond tool. The deep purple curve of Fig. 12(a) shows a peak at 1334 cm^{-1}. This line indicates that the diamond structure remained relatively intact after grinding-milling. Further, the graphite layer was removed gradually leaving a structure of sufficiently strong sp^3 bonds. Nose wear at the grinding-edge of the designed tool appears after grinding-milling (Fig. 12(b)). Nose wear, which occurs in the direction of the central axis of the grinding-milling tool (referring to Fig. 4(b)), is derived from abrasion. It

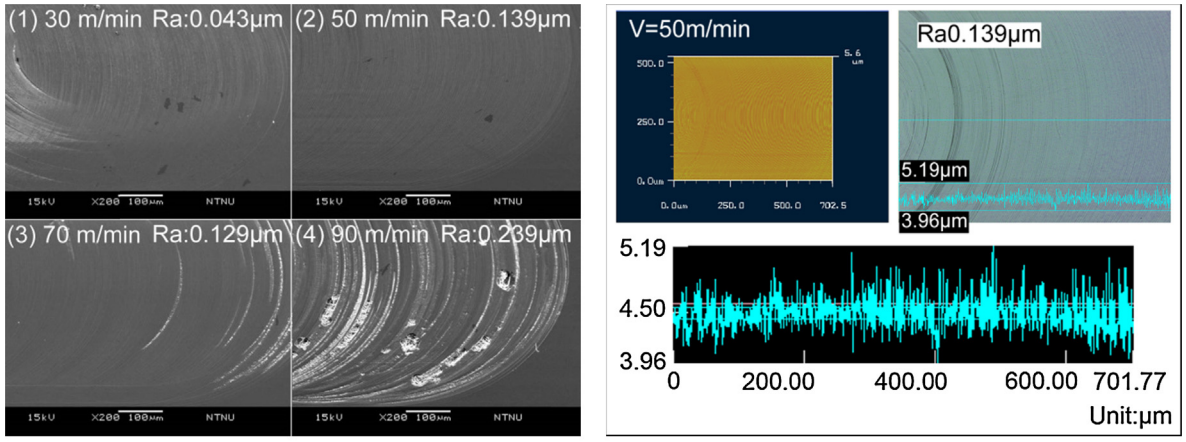

(a) Effect of grinding speed (b) Surface roughness at V=50 m/min

Fig. 11. Relationship between grinding speed and surface roughness.

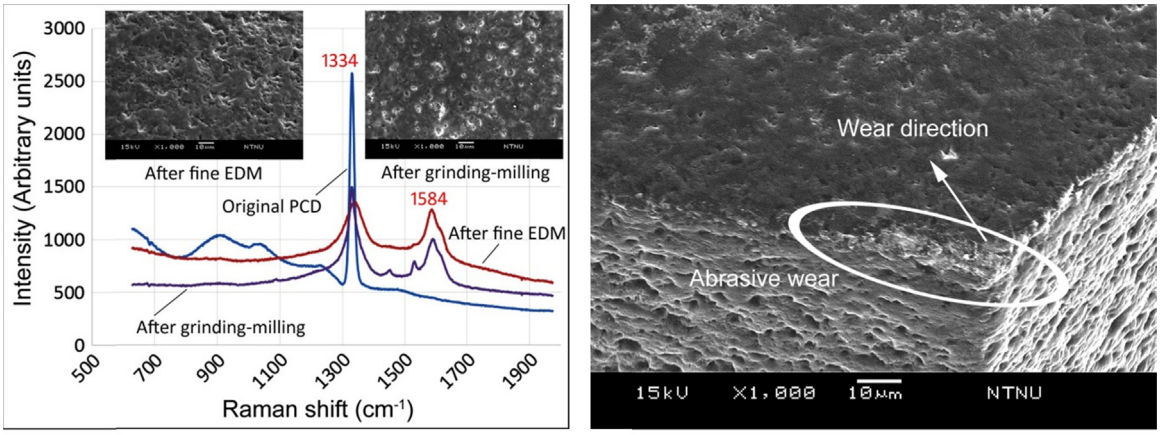

(a) Raman spectra in the used BD-PCD tool (b) Abrasive wear at the tool nose

Fig. 12. Graphitization and wear of the designed diamond tool.

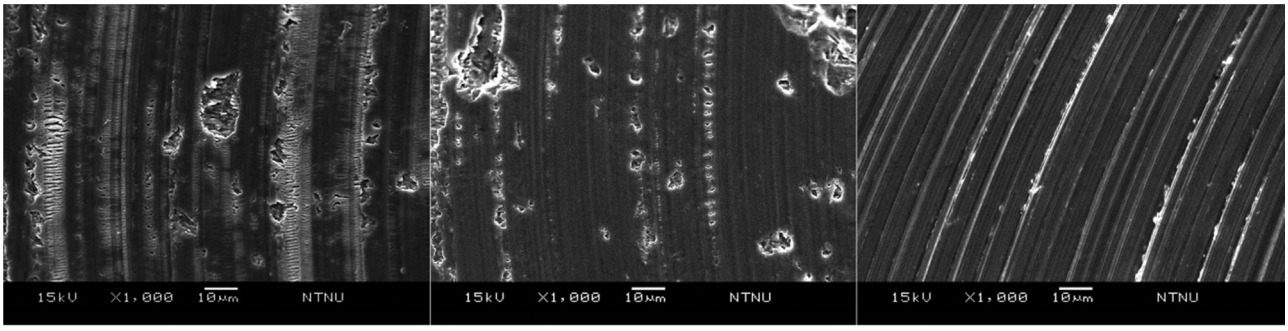

(a) Dry machining (b) Submerged machining (c) Oil-misted machining

Fig. 13. Effect of cooling operations.

occurs because of the scratching action of hard particles in the quartz glass. Protection against scratching is offered by the hard phases of the diamond tool. Result shows that a higher tool wear rate appears during the initial stage of grinding-milling. It is speculated that the degeneration layer and micro welding scars which adhere to the surface of the grinding-edge are ground away initially. Taylor's tool life equation ($VT^n = C$) (Taylor, 1907) is not suitable for the employed BD-PCD tool because it has multiple grinding edges. An estimation of tool life expectancy by the amount of consumption per unit length is proposed in this case. After this stage, an average wear rate of about 40 μm under a total path length of 3300 mm is found by SEM. The slow wear rate relates to the very shallow grinding depth (1 μm) used. More importantly, it can be ascribed to the design of a real-time feedback control mechanism, which creates an appropriately steady tool feed-rate for grinding-milling.

5.5. Effect of cooling operations

Reduction in tool wear can be accomplished by using a suitable lubricant and cooling during machining. These diminish friction and temperatures, thus decreasing tool wear. Due to grinding depth being controlled at <1 μm, damage from machining heat between tool and workpiece is less than that of friction resistance. Reducing friction is regarded as the most important factor in tool wear control. Three types of cooling operations: dry, submerged and oil-misted machining are employed during grinding-milling. Submerged machining involves the workpiece and tool being submerged in a coolant (normally EDM-oil) with a side flow of coolant. While oil-misted machining sprays a fine oil-mist onto the chip-tool interface using a high-pressure air tool to cool and lubricate the diamond tool. Brittle fracturing occurs in the operations of dry and submerged machining (see Fig. 13(a) and (b)). From this, it is inferred that the discharging of chips at the chip-tool interface is difficult due to the negative BRA used. As stated above, chips are repeatedly squeezing and scraping on the machined surface causing brittle fracturing even if the submerged operation increases lubrication. In contrast, the material removal mechanism is transferred to a ductile grinding regime when oil-misting is used (see Fig. 13(c)). Using oil-misting is more effective than just air cooling since micro oil-droplets can be supplied to the tool-chip interface (Obikawa et al., 2009) to reduce friction. Besides which, chips are swiftly blown away by the high-pressure air.

6. Conclusions

An intellectualized feedback mechanism is used to successfully micromachine quartz glass in this study. The original bench-type machine tool provides grinding depth down to the level of several nanometers, realizing ductile regime machining on quartz glass. A feedback control loop design facilitates corrects the feed-rate of the tool, creating a proper steady grinding-milling force to protect the quartz glass against brittle fracturing. How the self-learning mechanism works is carefully examined and verified in the manufacture of a miniaturized 3-D step pyramid on quartz glass. Both quantitative and qualitative studies of the grinding-milling process are conducted to provide a complete set of information on the manufacturing process. It is expected that the technique could be extended to high-precision turning, milling and grinding, as well

as related processes in the electro-optical industry of the future. Below is a summary of the results:

- A micro end grinding-tool, possessing a negative BRA to allow for machining by compressive stress, is designed so that quartz glass grinding avoids fracturing due to tensile stress.
- w-EDM is utilized to form a diamond tool made of BD-PCD. The effect of spark erosion at the interface of PCD and the tungsten carbide substrate is studied to prevent notch circles from occurring.
- The grinding-milling force can be monitored in real-time using sensitized load cells that feedback to the milling tool to ensure a steady and appropriate feed-rate.
- Experimental results indicate that the optimum grinding depth and milling speed are 1 μm and 50–70 m/min, respectively, the corresponding grinding-milling force and surface roughness are 0.4 N and Ra0.056 μm, respectively.
- Oil-misted machining allows micro oil-droplets to penetrate the tool-chip interface, reducing friction. A low wear rate for BD-PCD versus quartz glass is 40 μm in a total path length of 3300 mm.

Acknowledgements

The authors would like to thank the National Science Council of the Republic of China, Taiwan, for financially supporting this study under Contract No. NSC 102-2218-E-003-001-MY2 and FINE ABRASIVES TAIWAN CO., LTD. for supplying the BD-PCD samples. Their assistance is gratefully acknowledged.

References

Aerotech, Inc, 2012. ANT95-XY BASE & PLUS Mechanical-Bearing Direct-Drive XY Linear Stage. http://www.aerotech.com

Amitay, G., Malkin, S., Koren, Y., 1981. Adaptive control optimization of grinding. Trans. ASME 103, 131–136.

Astakhov, V.P., 1999. A treatise on material characterization in the metal cutting process. Part 2: Cutting as the fracture of workpiece material. J. Mater. Process. Technol. 96, 34–41.

Bifano, T.G., Dow, T.A., Scattergood, R.O., 1991. Ductile-regime grinding: a new technology for machining brittle materials. Trans. ASME 113, 184–189.

Blackley, W.S., Scattergood, R.O., 1991. Ductile regime model for diamond turning of brittle materials. Precis. Eng. 13, 95–103.

Chen, S.T., Chang, C.H., 2013. Development of an ultrathin BD-PCD wheel-tool for in situ microgroove generation on NAK80 mold steel. J. Mater. Process. Technol. 213, 740–751.

Chen, S.T., Jiang, Z.H., Wu, Y.Y., Yang, H.Y., 2011. Development of a grinding-drilling technique for holing optical grade glass. Int. J. Mach. Tools Manuf. 51, 95–103.

Deng, J., Zhang, H., Wu, Z., Liu, A., 2011. Friction and wear behavior of polycrystalline diamond at temperatures up to 700 °C. Int. J. Refract. Met. Hard Mater. 29, 631–638.

Dubey, A.K., Yadava, V., 2008. Laser beam machining—a review. Int. J. Mach. Tools Manuf. 48, 609–628.

Ekimov, E.A., Sidorov, V.A., Bauer, E.D., Mel'nik, N.N., Curro, N.J., Thompson, J.D., Stishov, S.M., 2004. Superconductivity in diamond. Nature 428, 542–545.

Guzzo, P.L., Raslan, A.A., De Mello, J.D.B., 2003. Ultrasonic abrasion of quartz crystals. Wear 255, 67–77.

Hildebrand, J., Hecht, K., Bliedtner, J., Müller, H., 2012. Advanced analysis of laser beam polishing of quartz glass. Phys. Procedia 39, 277–285.

Hock, K., Adelmann, B., Hellmann, R., 2012. Comparative study of remote fiber laser and water-jet guided laser cutting of thin metal sheets. Phys. Procedia 39, 225–231.

Jain, V.K., Adhikary, S., 2008. On the mechanism of material removal in electrochemical spark machining of quartz under different polarity conditions. J. Mater. Process. Technol. 200, 460–470.

Kalish, R., 2001. The search for donors in diamond. Diam. Relat. Mater. 10, 1749–1755.

Moriyoshi, Y., Kamo, M., Setaka, N., Sato, Y., 1982. The microstructure of natural polycrystal diamond, carbonado and ballas. J. Mater. Sci. 18, 217–224.

Obikawa, T., Asano, Y., Kamata, Y., 2009. Computer fluid dynamics analysis for efficient spraying of oil mist in finish-turning of Inconel 718. Int. J. Mach. Tools Manuf. 49, 971–978.

Sommer, C., 2000. Non-traditional Machining Handbook. Advance Publishing, Inc., Houston, pp. 117–124.

Sung, C.M., Tai, M.F., 1997. Reactivities of transition metals with carbon: implications to the mechanism of diamond synthesis under high pressure. Int. J. Refract. Met. Hard Mater. 15, 237–256.

Suzuki, K., Shiraishi, Y., Nakajima, N., Iwai, M., Ninomiya, S., Tanaka, Y., Uematsu, T., 2009. Development of new PCD made up of boron doped diamond particles and its machinability by EDM. Adv. Mater. Res. 76–78, 684–689.

Taylor, F.W., 1907. On the art of cutting metals. Trans. ASME 28, 31–58.